

Supporting Information

Periodic Arrays of Phosphorene Nanopores as Antidot Lattices with Tunable Properties

Andrew Cupo,^{1#} Paul Masih Das,^{2#} Chen-Chi Chien,² Gopinath Danda,^{2,3} Neerav Kharche,¹ Damien Tristant,¹ Marija Drndić,^{2*} and Vincent Meunier^{1*}

¹Department of Physics, Applied Physics, and Astronomy, Rensselaer Polytechnic Institute, Troy, New York, 12180, USA

²Department of Physics and Astronomy, University of Pennsylvania, Philadelphia, Pennsylvania, 19104, USA

³Department of Electrical and Systems Engineering, University of Pennsylvania, Philadelphia, Pennsylvania, 19104, USA

[#]These authors contributed equally to this work.

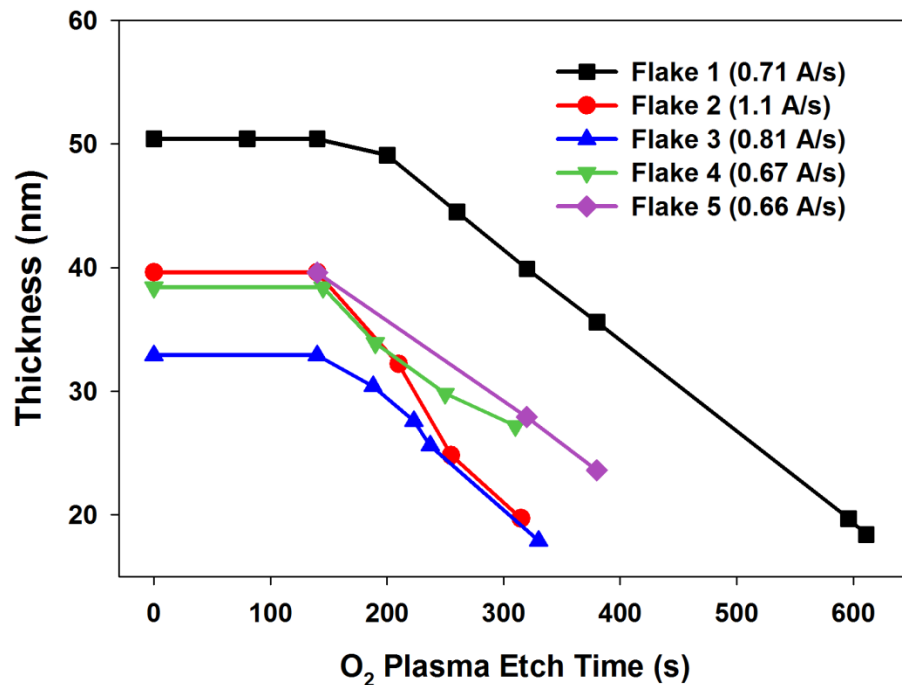
*To whom correspondence should be addressed: drndic@physics.upenn.edu and meuniv@rpi.edu

Table of Contents:

- 1. Plasma etch rates for few-layer black phosphorus**
- 2. Additional Raman maps for fabricated antidot arrays**
- 3. All atomic models of optimized H-passivated PALs**
- 4. Geometric parameters of PALs**
- 5. Edge energy differences**
- 6. All DOS and PDOS edge/interior plots**
- 7. Computations of the band gap**
- 8. Band gap limiting charge density**
- 9. All spatial distributions of the band gap**
- 10. Calculated power spectra**
- 11. Justification for neglecting spin-polarization**

Section S1: Plasma etch rates for few-layer black phosphorus

Thickness of few-layer black phosphorus flakes measured with atomic force microscopy (AFM) during oxygen (O_2) plasma thinning (150 W, 30 sccm, 45 mTorr). The zero slope region corresponds to the formation of an oxide passivation layer followed by a constant period of layer-by-layer etching at a rate of ~1 layer per 10 seconds (0.66-1.1 Å/s). Using concurrent Raman and AFM measurements, the thickness of this capping oxide layer was seen to remain constant (17 nm) during the layer-by-layer etching procedure, consistent with previous reports. An error of ± 1 nm is attributed to each point due to surface roughness and instrument resolution.



Section S2: Additional Raman maps for fabricated antidot arrays

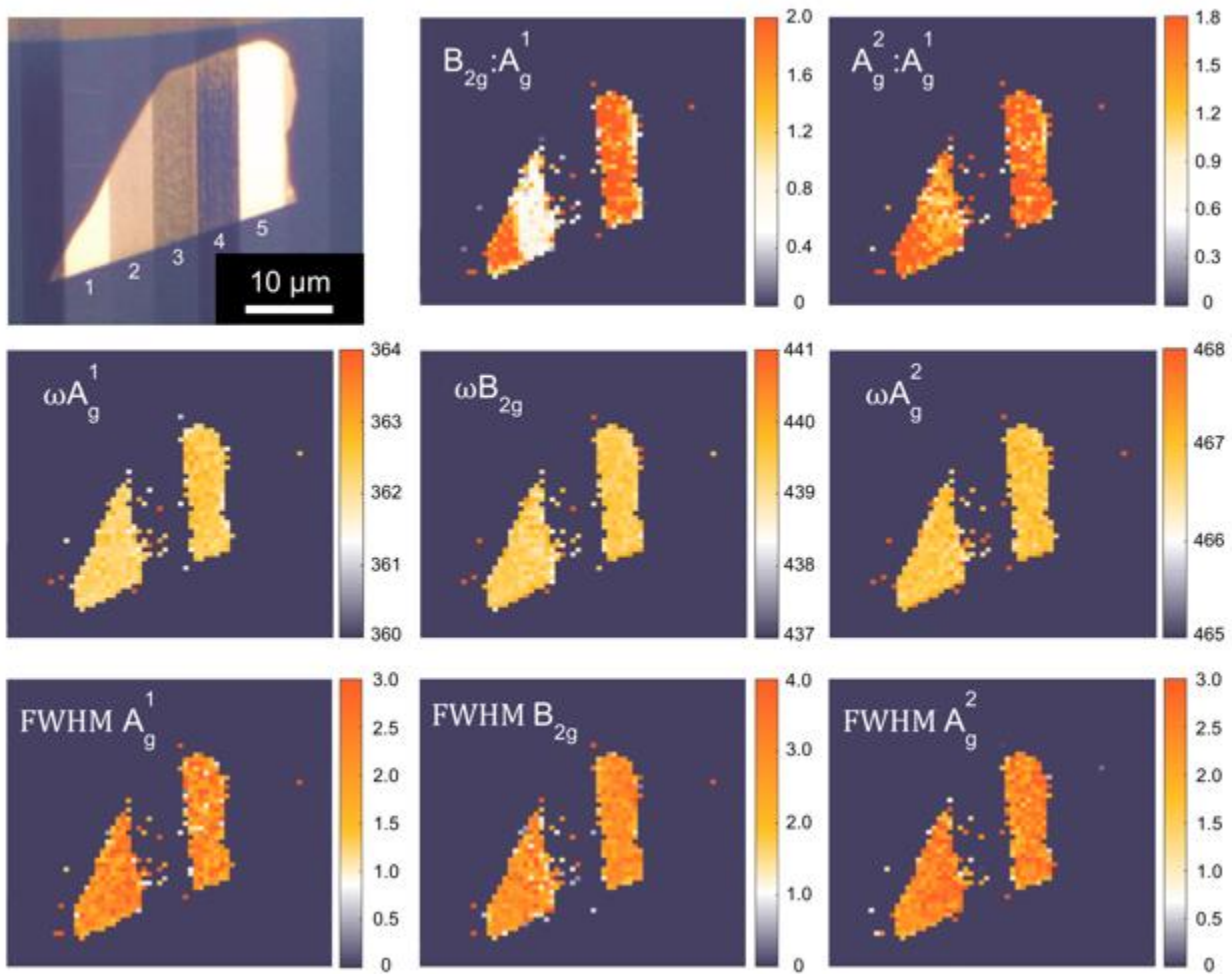


Figure S2.1. First row (left to right): optical image, $B_{2g}:A_g^1$ intensity Raman map, and $A_g^2:A_g^1$ intensity Raman map of the patterned few-layer BP flake from Figure 2 of the main text. Middle row (left to right): A_g^1 , B_{2g} , and A_g^2 peak frequencies (ω) for the same flake, showing no discernible Raman shifts. Bottom row (left to right): A_g^1 , B_{2g} , and A_g^2 peak full widths at half maximum (FWHM).

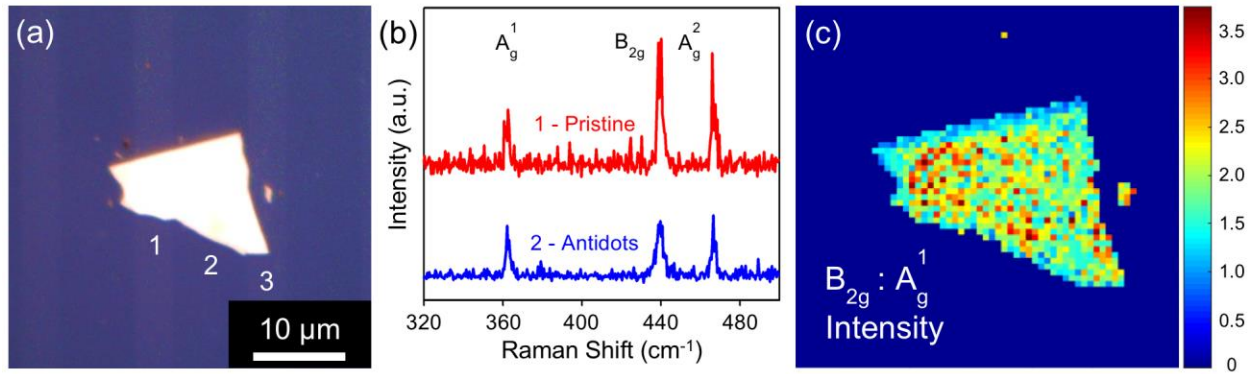
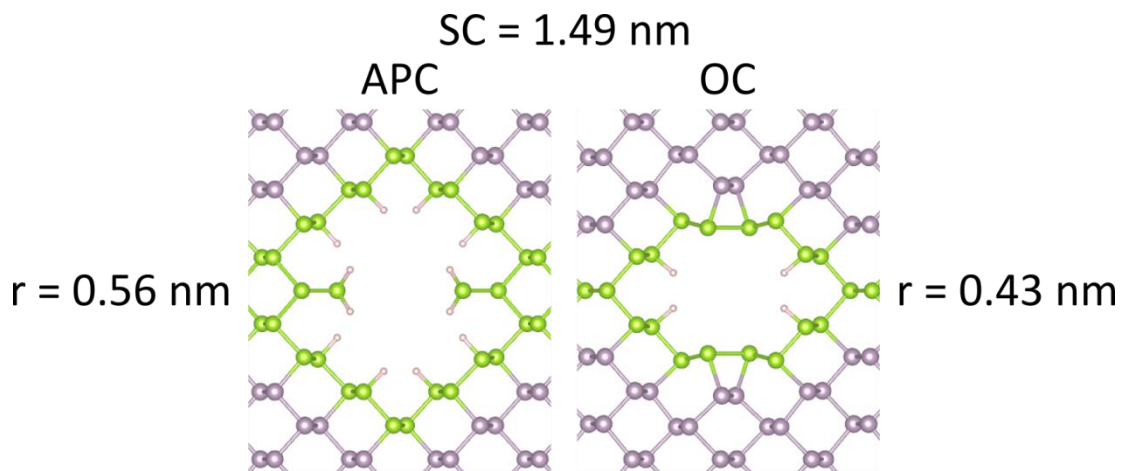


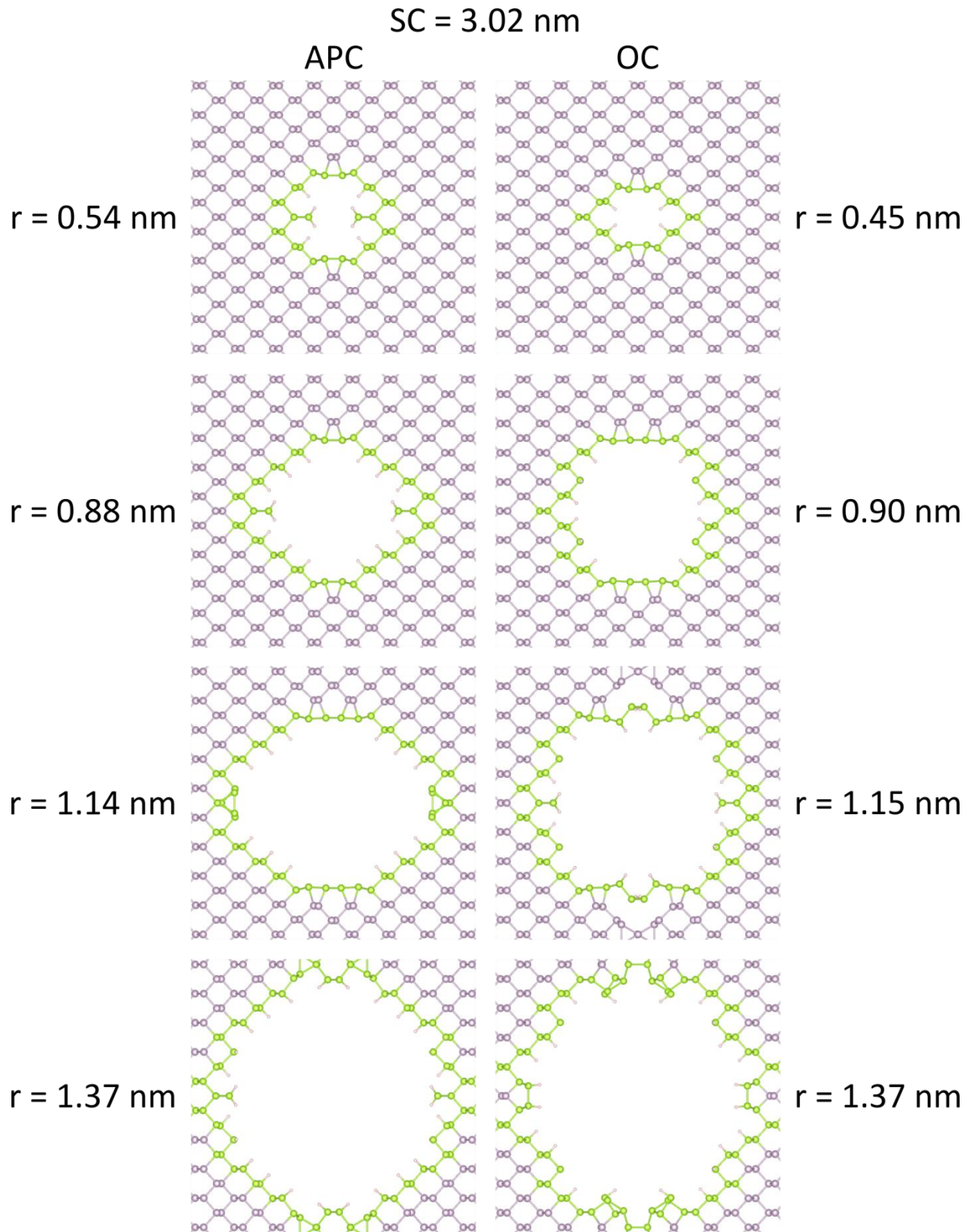
Figure S2.2. (a) Optical image of columnar regions with (1), (3) pristine few-layer BP and (2) patterned antidots (SC = 65 nm r = 13 nm). (b) Raman spectra of regions (1) and (2) normalized to the A_g¹ peak of (1) and (c) B_{2g}:A_g¹ intensity Raman map from the sample in (a) showing, in this case, in-plane B_{2g} phonon suppression.

Section S3: All atomic models of optimized H-passivated PALs

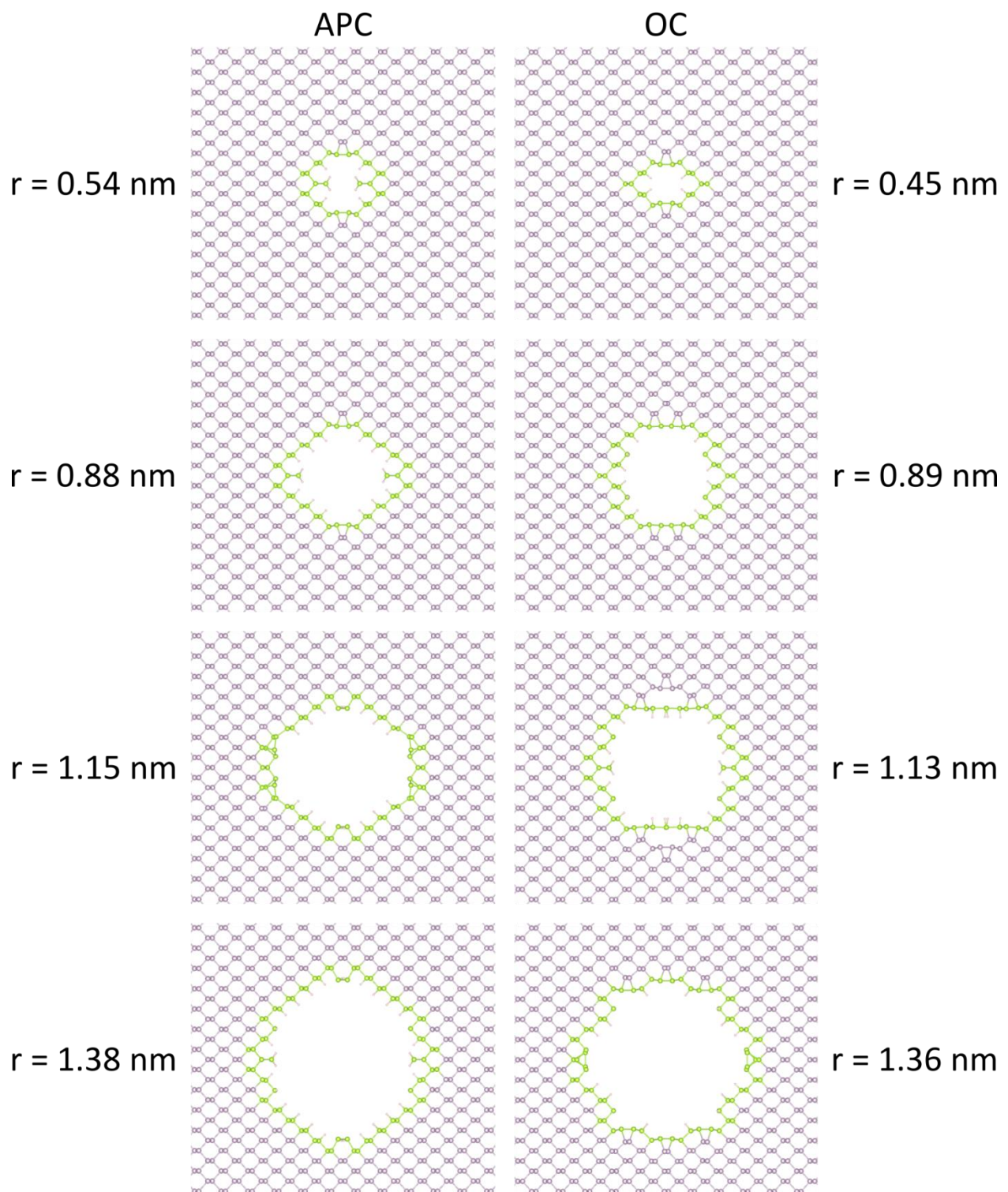
Note: Rows of atoms across from each other on the edges of the antidot unit cell are equivalent.

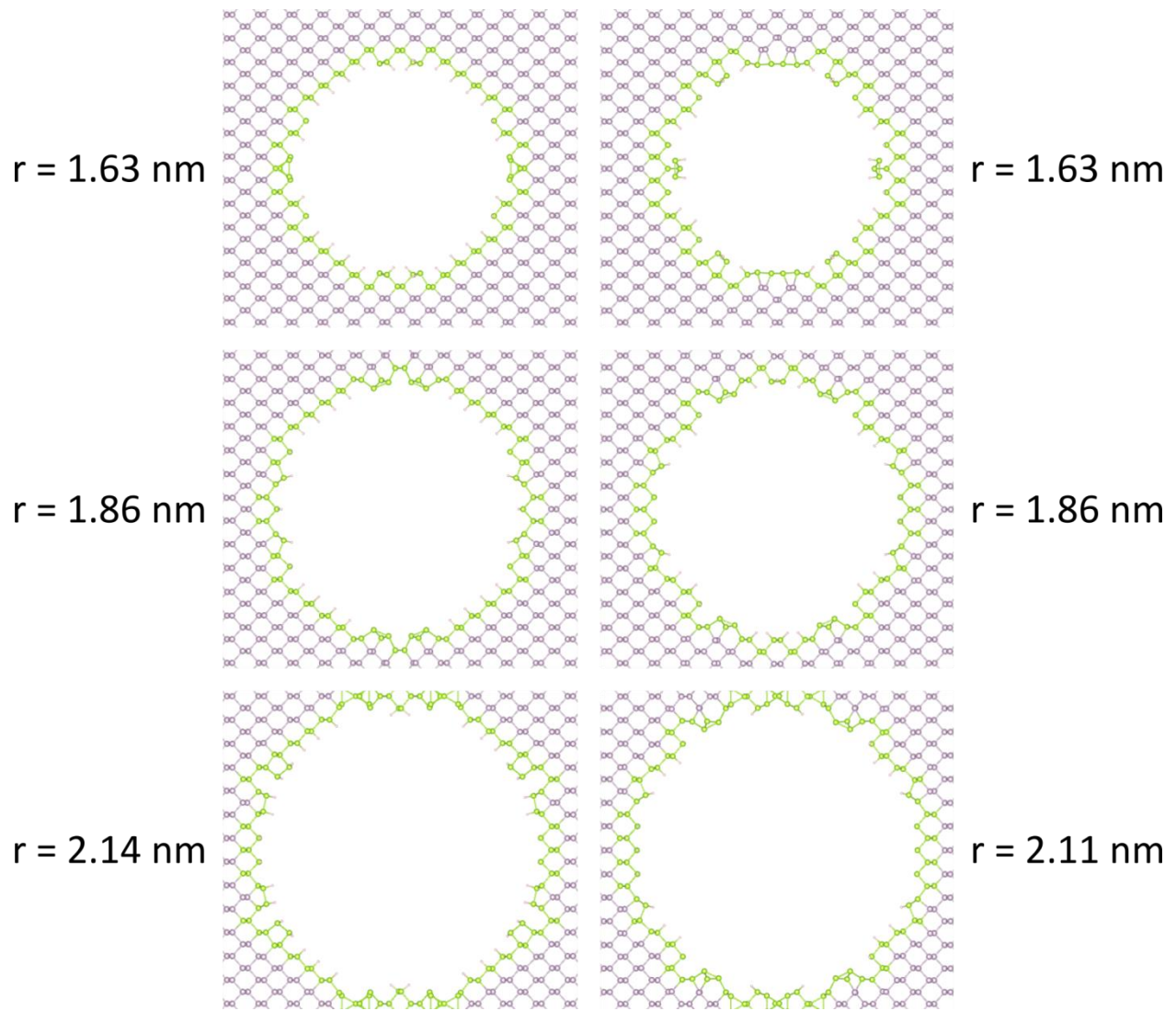
(Edge = Green and Interior = Purple)





$SC = 4.56 \text{ nm}$



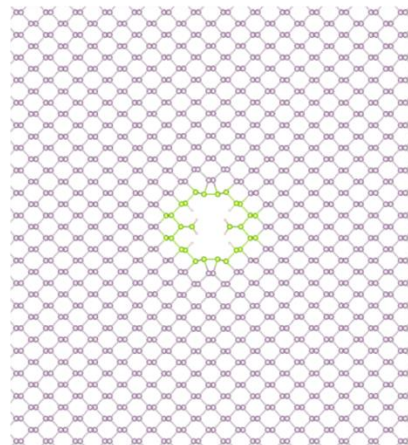


$SC = 5.99 \text{ nm}$

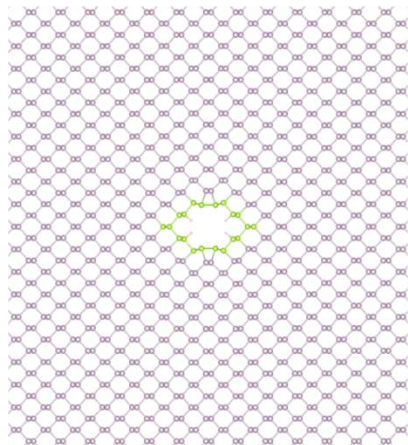
APC

OC

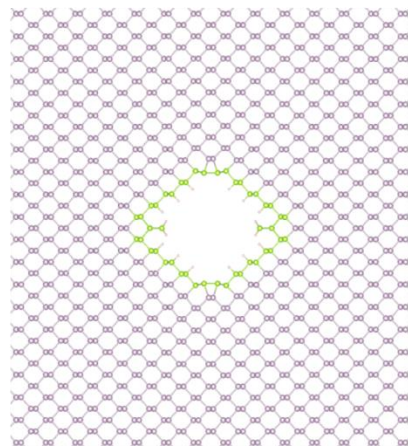
$r = 0.54 \text{ nm}$



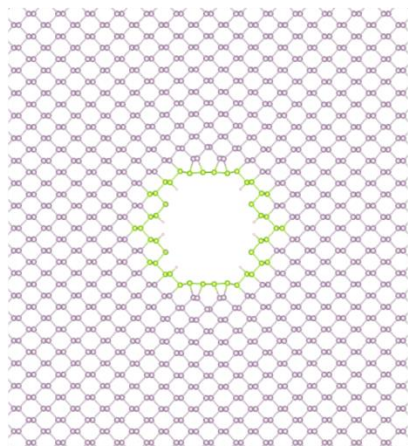
$r = 0.45 \text{ nm}$



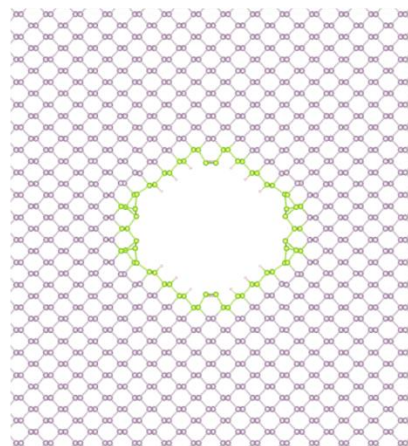
$r = 0.88 \text{ nm}$



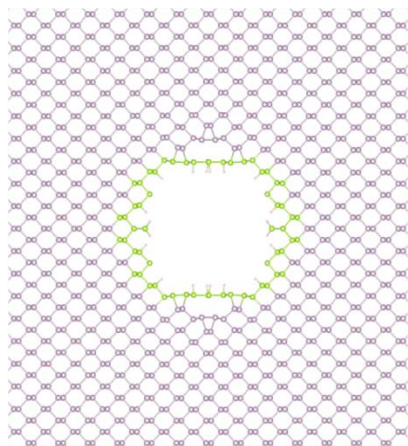
$r = 0.89 \text{ nm}$

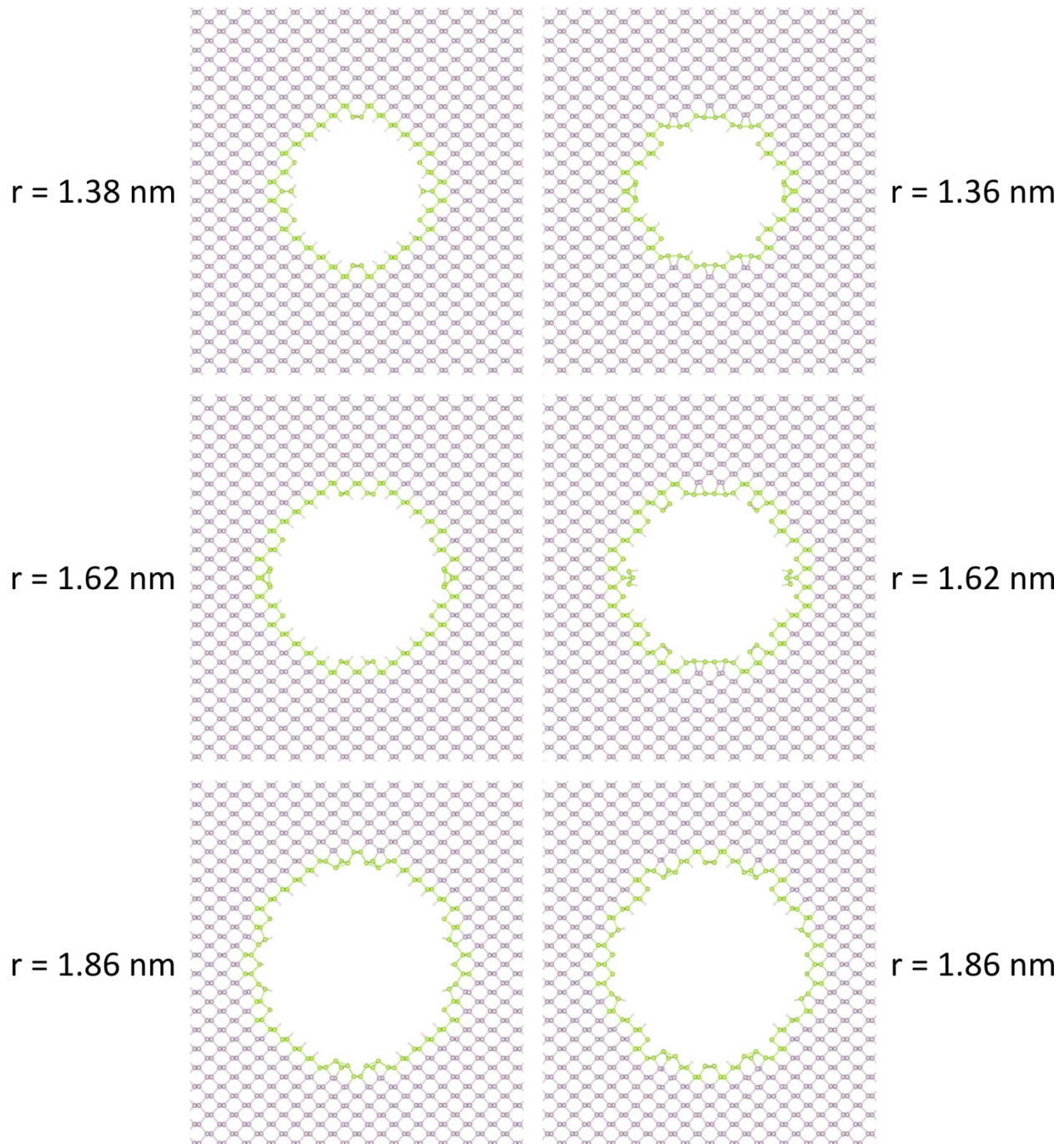


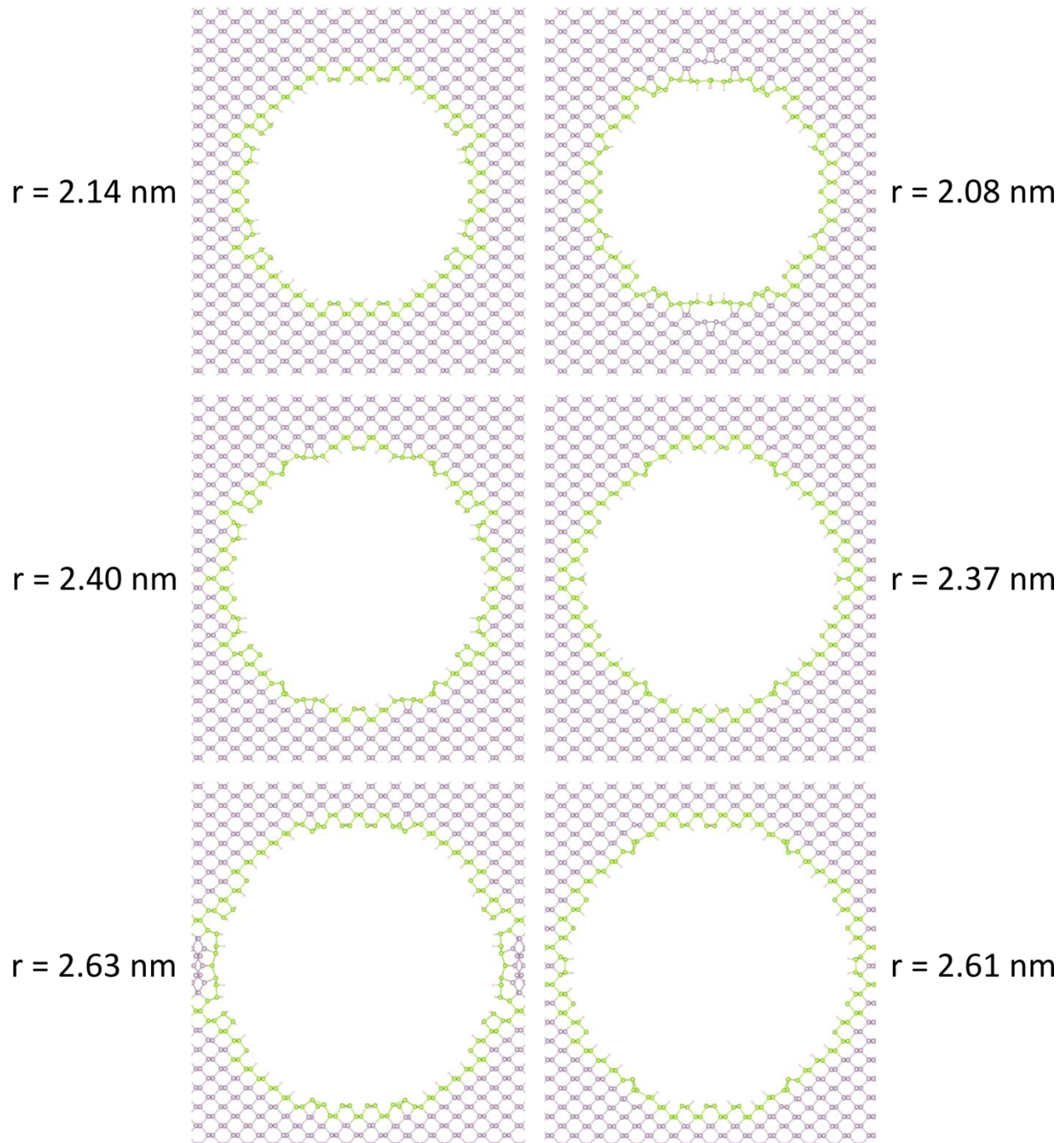
$r = 1.15 \text{ nm}$



$r = 1.13 \text{ nm}$







Section S4: Geometric parameters of PALs

All dimensions are given in units of nm

X: armchair

Y: zigzag

Symbol Legend

UC_x : Number of phosphorene unit cells along x

SC_x : X superlattice constant

UC_y : Number of phosphorene unit cells along y

SC_y : Y superlattice constant

SC : Average in-plane superlattice constant

r_s : Radius of hole set in initial geometry generation script

r_{PAL} : Radius of the finalized antidot geometry, calculated as the average radius of all phosphorus edge atoms

SD_r : Standard deviation in the above radius calculated as

$$SD_r = \sqrt{VAR_r} = \sqrt{\frac{1}{n_{edge}} \sum_{i=1}^{n_{edge}} (r_i - r_{PAL})^2},$$

where r_i is the radius of the i th edge atom and n_{edge} is the total number of edge atoms

Supercell Parameters

UC_x	SC_x	UC_y	SC_y	$SC = (SC_x + SC_y) / 2$
3	1.31	5	1.66	1.49
7	3.05	9	2.99	3.02
11	4.80	13	4.32	4.56
13	5.67	19	6.32	5.99

APC $SC = 1.49$ nm

r_s	r_{PAL}	SD_r
0.375	0.56	0.09

OC $SC = 1.49$ nm

r_s	r_{PAL}	SD_r
0.375	0.43	0.08

APC $SC = 3.02$ nm

r_s	r_{PAL}	SD_r
0.375	0.54	0.10
0.75	0.88	0.11
1	1.14	0.12
1.25	1.37	0.08

OC $SC = 3.02$ nm

r_s	r_{PAL}	SD_r
0.375	0.45	0.10
0.75	0.90	0.09
1	1.15	0.11
1.25	1.37	0.10

APC $SC = 4.56$ nm

r_s	r_{PAL}	SD_r
0.375	0.54	0.10
0.75	0.88	0.11
1	1.15	0.10
1.25	1.38	0.09
1.5	1.63	0.09
1.75	1.86	0.08
2	2.14	0.11

OC $SC = 4.56$ nm

r_s	r_{PAL}	SD_r
0.375	0.45	0.10
0.75	0.89	0.09
1	1.13	0.11
1.25	1.36	0.11
1.5	1.63	0.13
1.75	1.86	0.10
2	2.11	0.10

APC $SC = 5.99$ nm

r_s	r_{PAL}	SD_r
0.375	0.54	0.10
0.75	0.88	0.11
1	1.15	0.10
1.25	1.38	0.09
1.5	1.62	0.09
1.75	1.86	0.08
2	2.14	0.11
2.25	2.40	0.11
2.5	2.63	0.11

OC $SC = 5.99$ nm

r_s	r_{PAL}	SD_r
0.375	0.45	0.10
0.75	0.89	0.09
1	1.13	0.11
1.25	1.36	0.10
1.5	1.62	0.12
1.75	1.86	0.10
2	2.08	0.10
2.25	2.37	0.11
2.5	2.61	0.09

Section S5: Edge energy differences

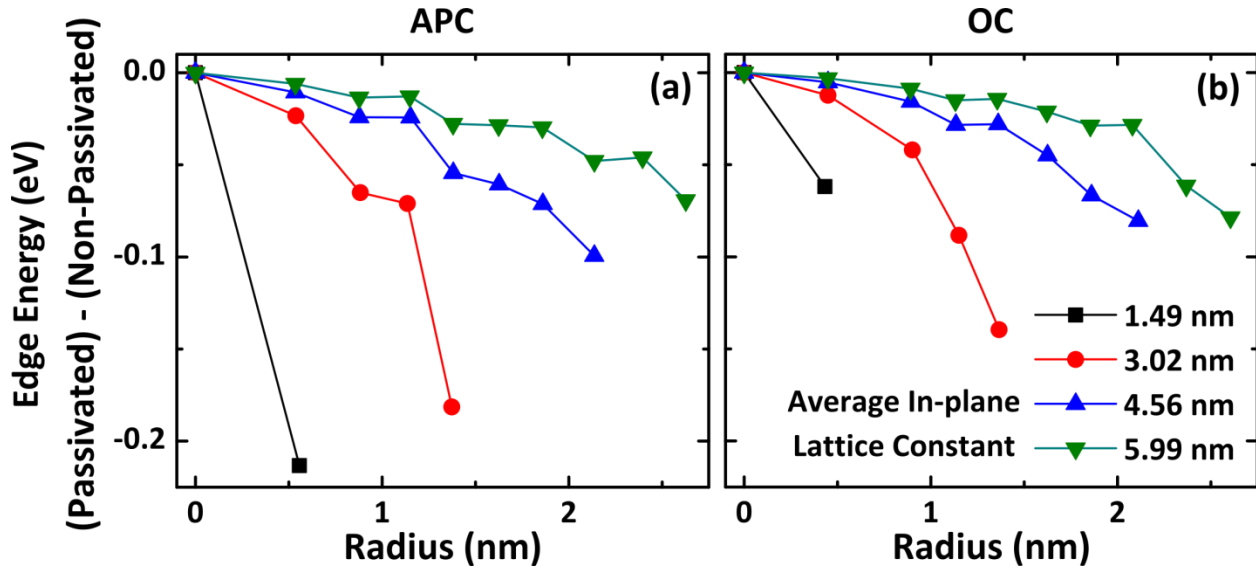


Figure S5.1. Edge energy given as the difference (passivated) – (non-passivated). (a) APC. (b) OC. For all antidot structures the result is negative, which indicates that passivating the edge with H atoms stabilizes all structures.

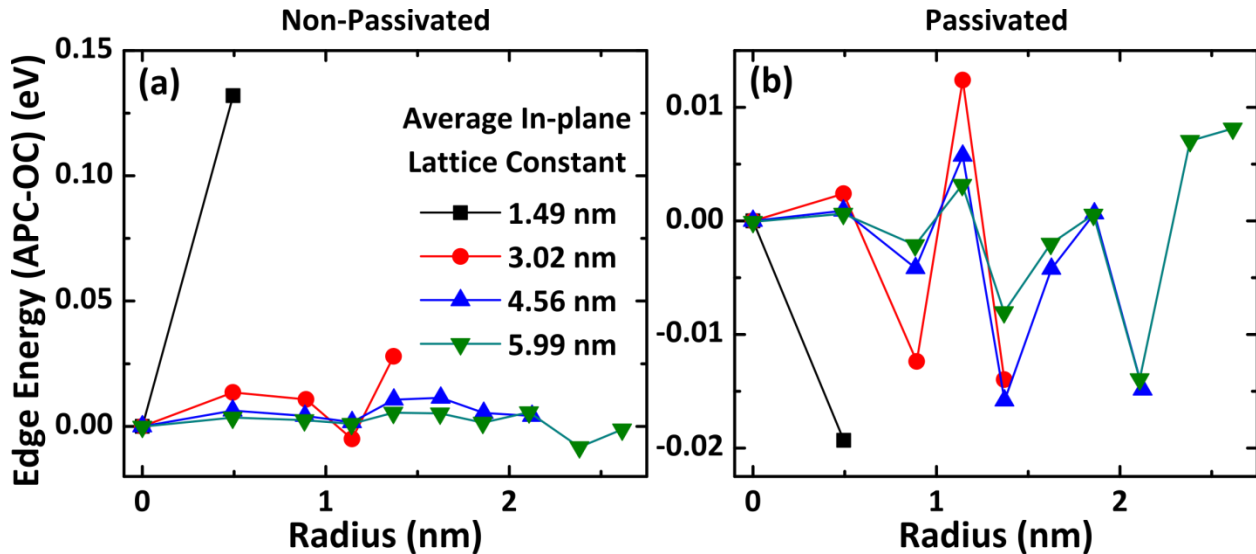
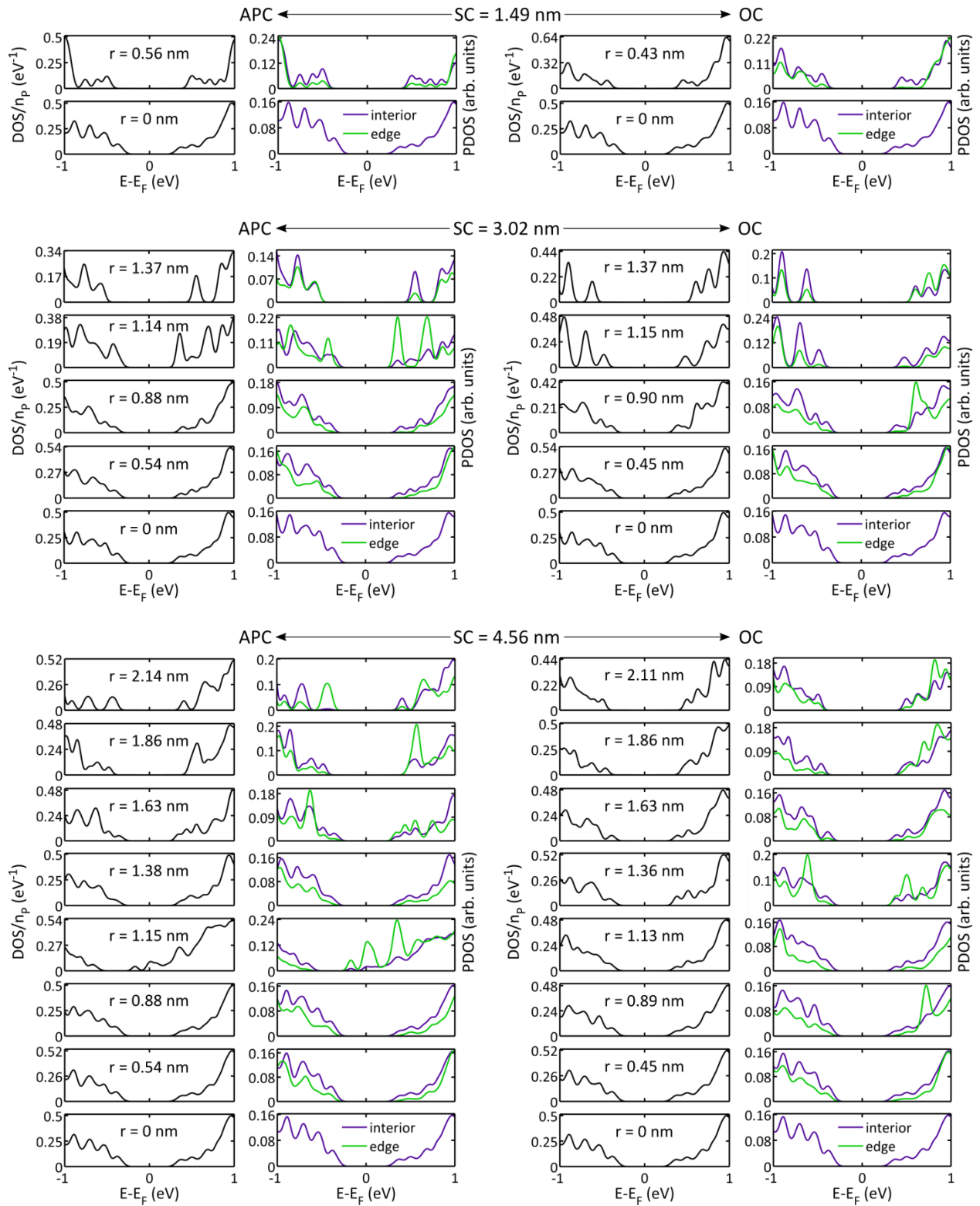
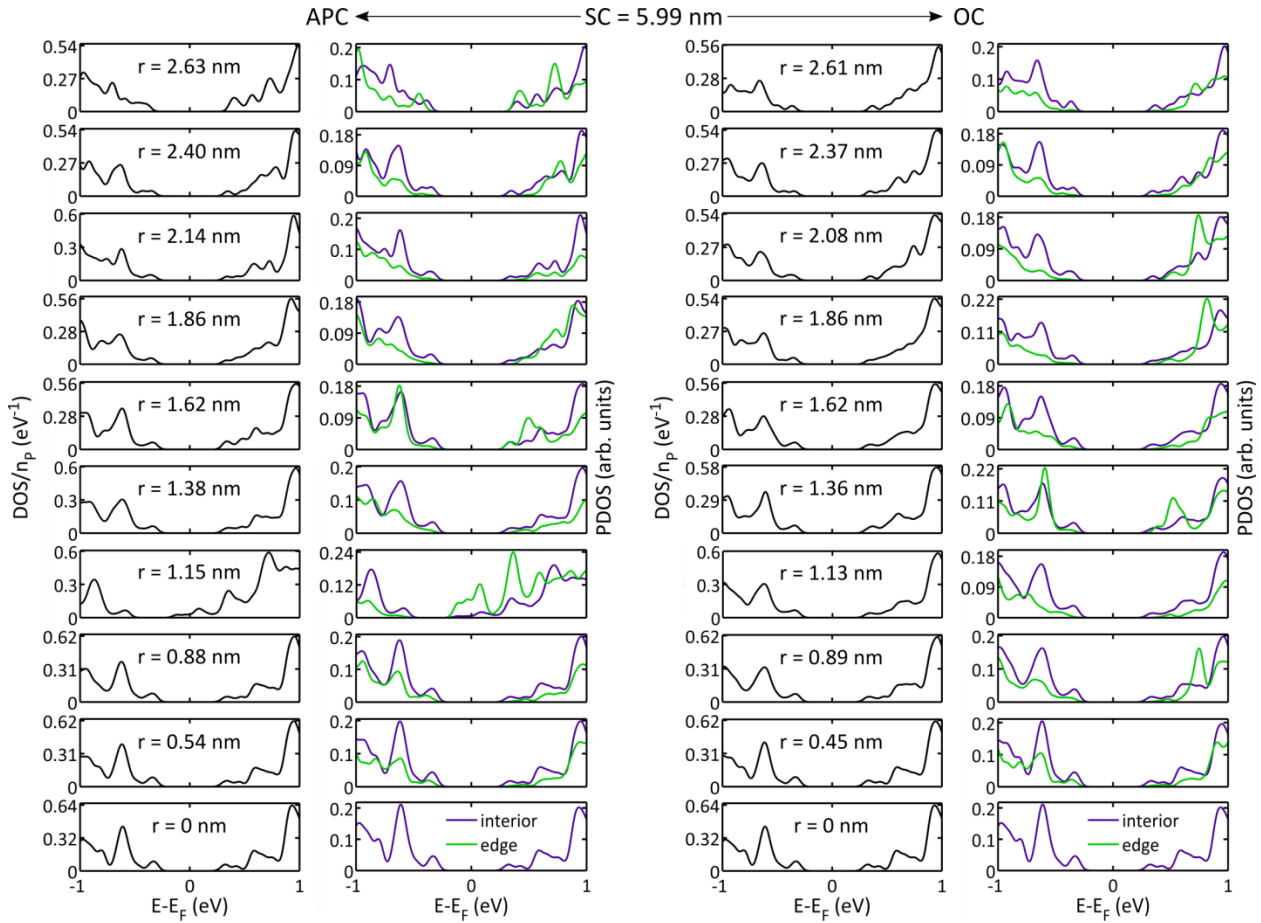


Figure S5.2. Edge energy given as the difference between corresponding (same supercell size and nearly the same radius) APC and OC structures. The horizontal axis is the average radius between the structures.

Section S6: All DOS and PDOS edge/interior plots





Section S7: Computations of the band gap

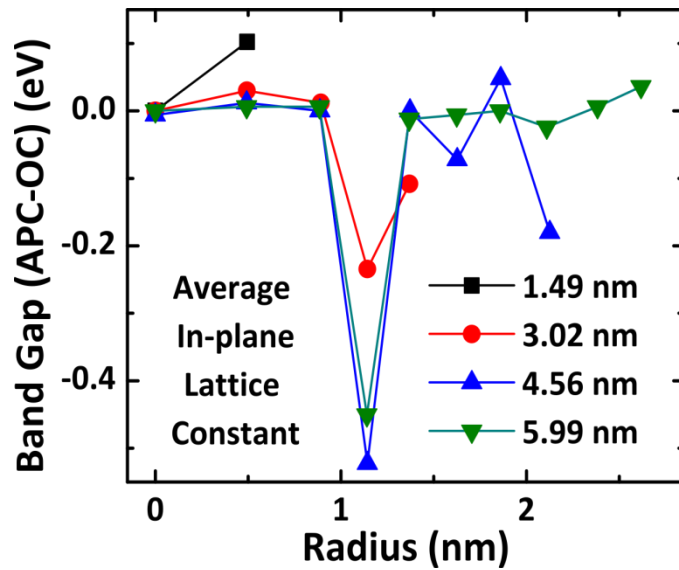


Figure S7.1. Band gap difference between corresponding APC and OC PALs.

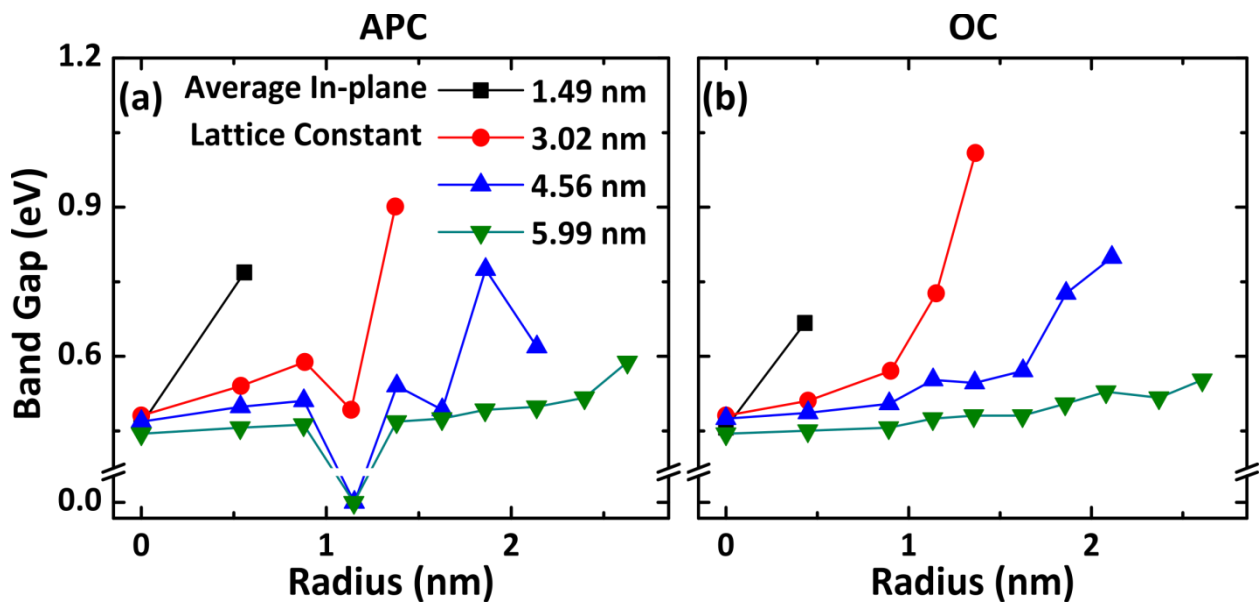


Figure S7.2 Band gap for PALs calculated using the total phosphorus PDOS. (a) APC. (b) OC.

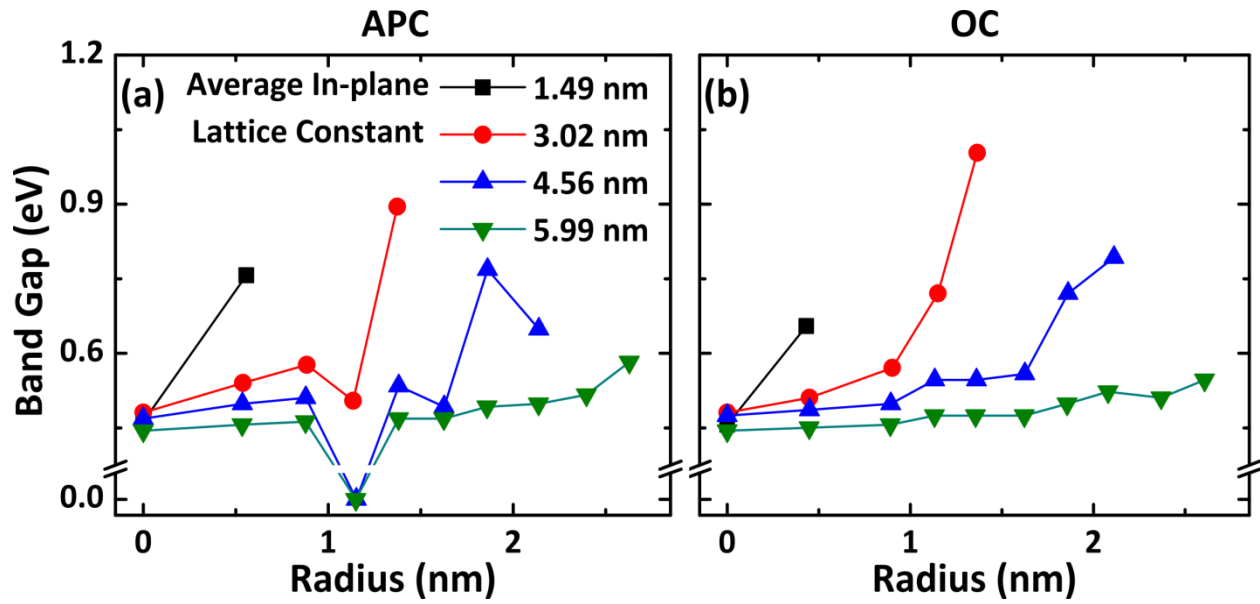
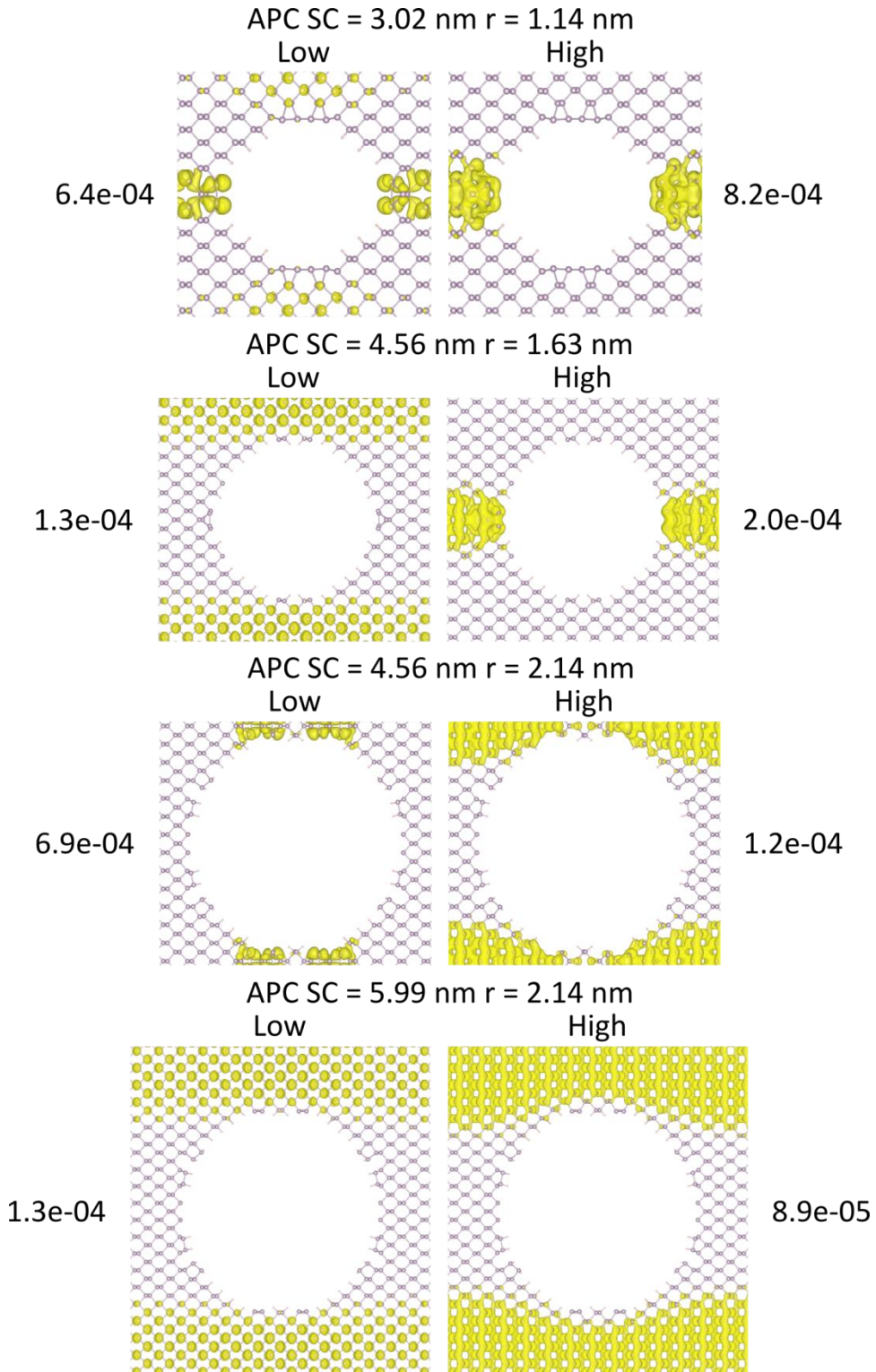
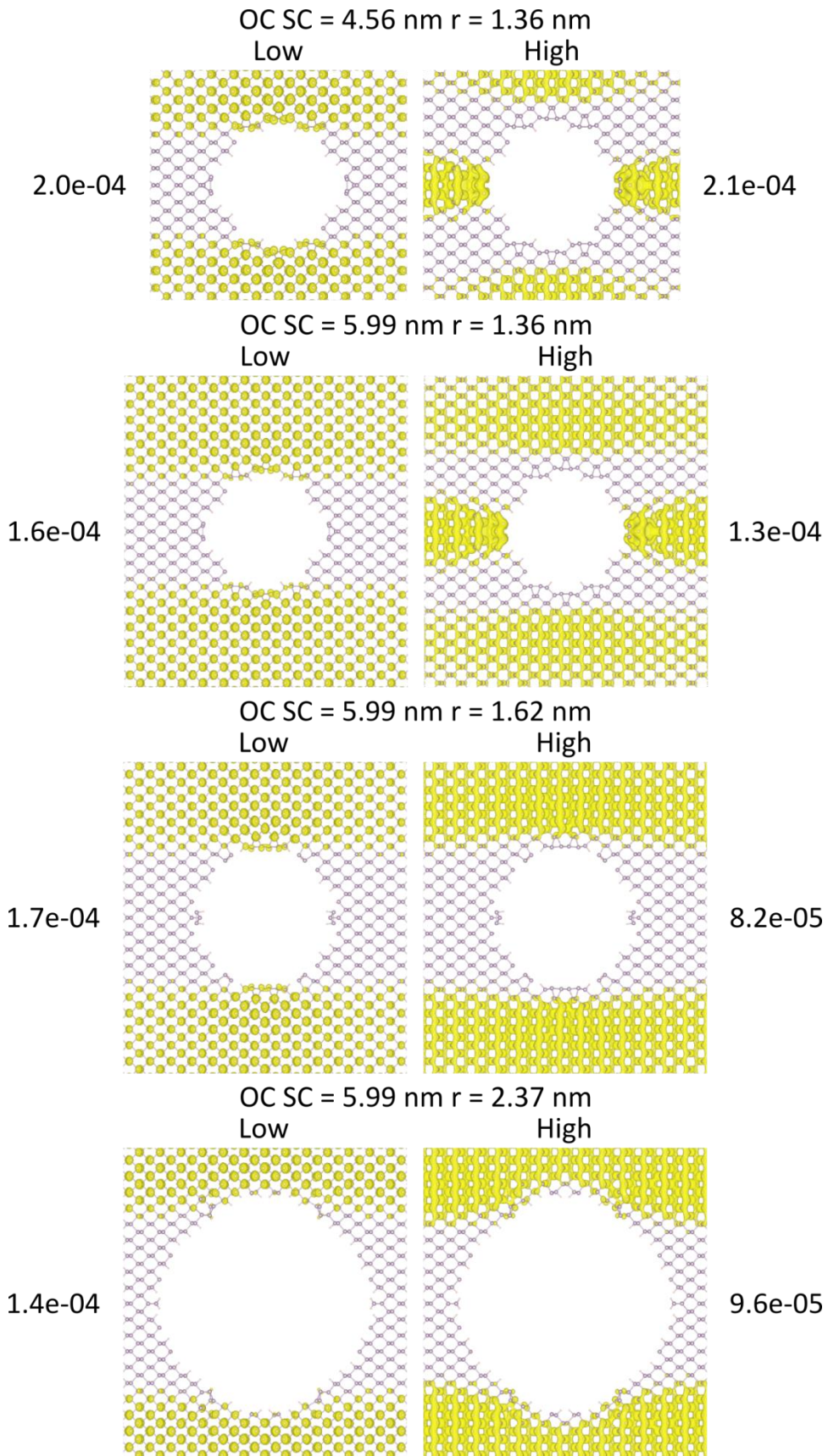


Figure S7.3 Band gap for PALs calculated using the phosphorus interior PDOS. (a) APC. (b) OC.

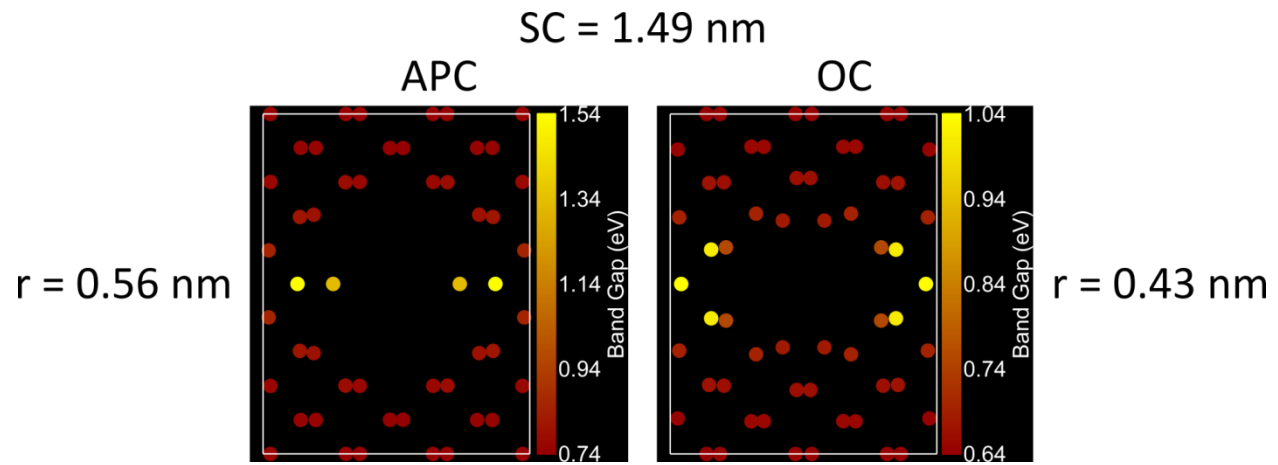
Section S8: Band gap limiting charge density

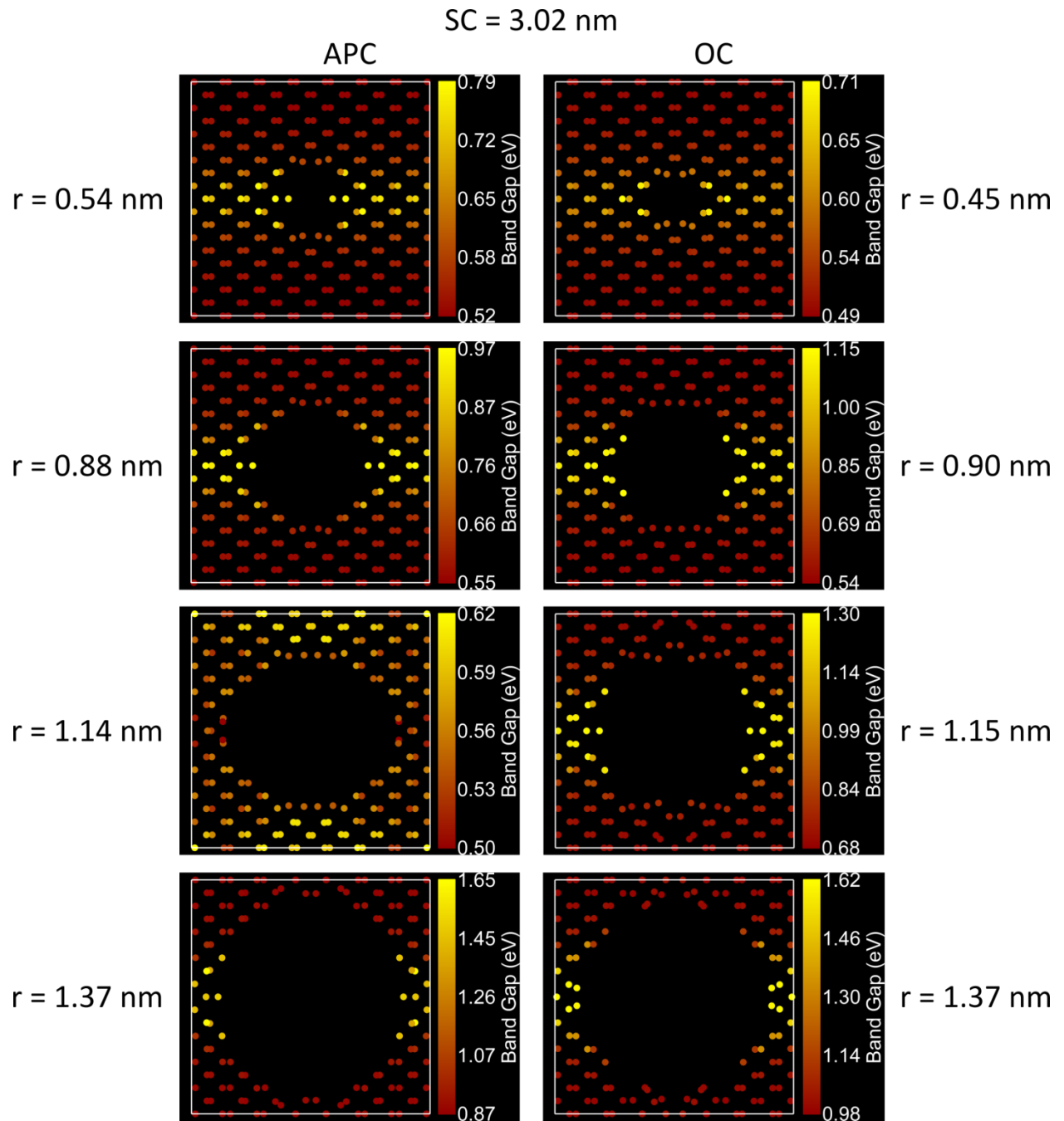
Isosurface values given in units of a_0^{-3} , where a_0 is the Bohr radius.

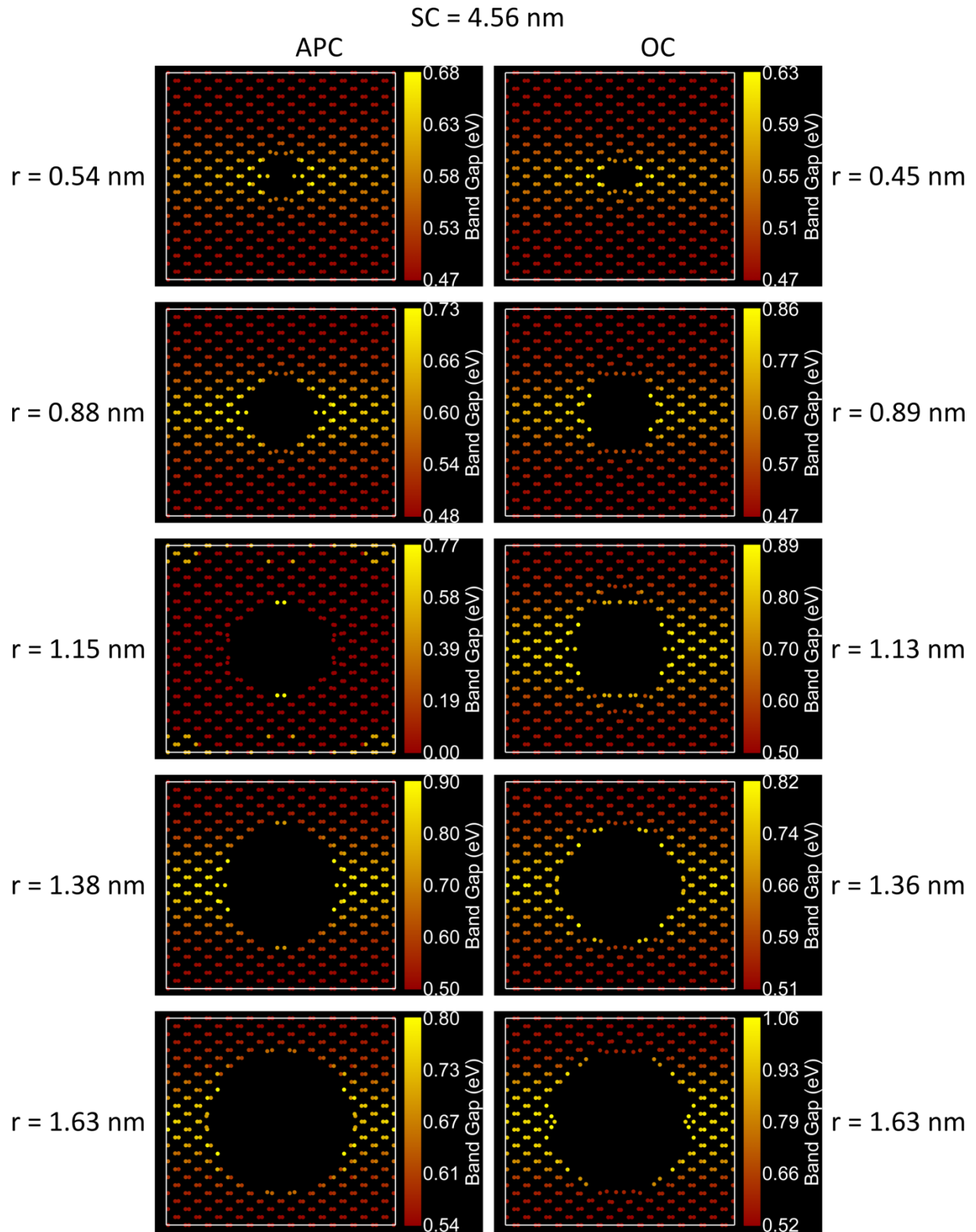


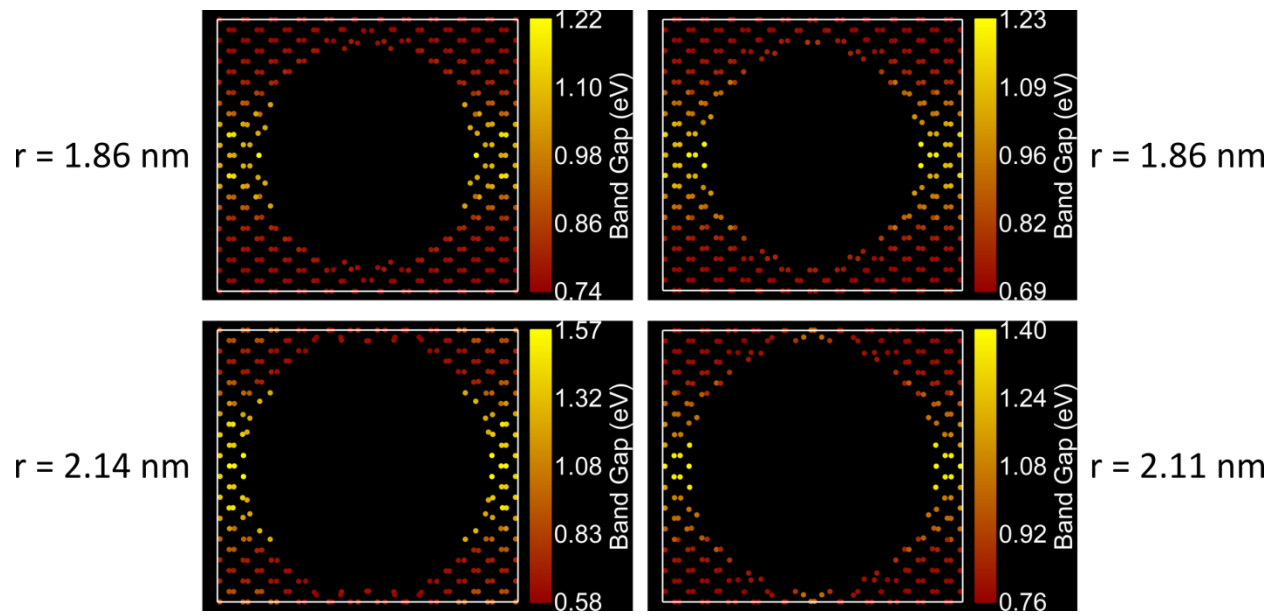


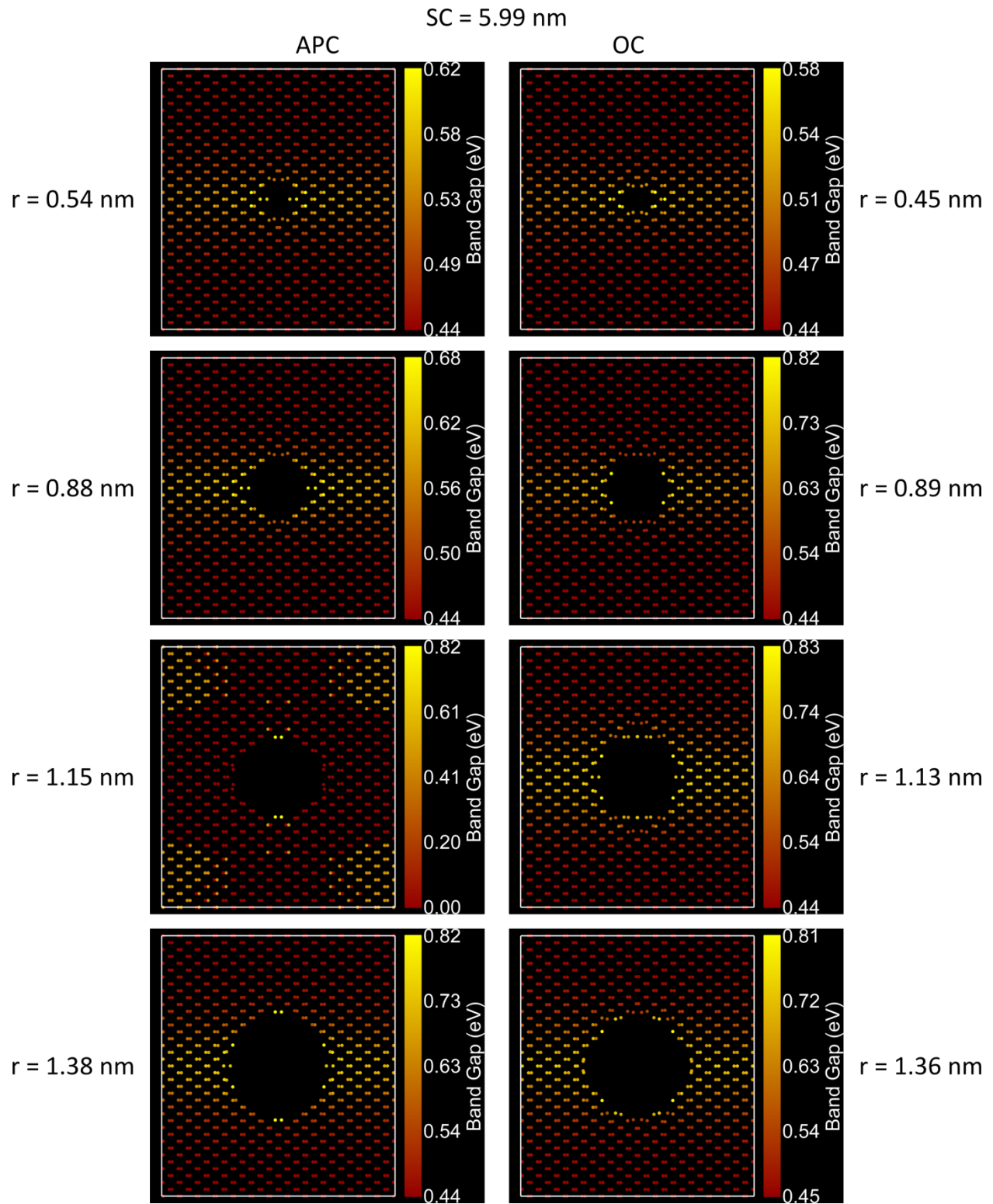
Section S9: All spatial distributions of the band gap

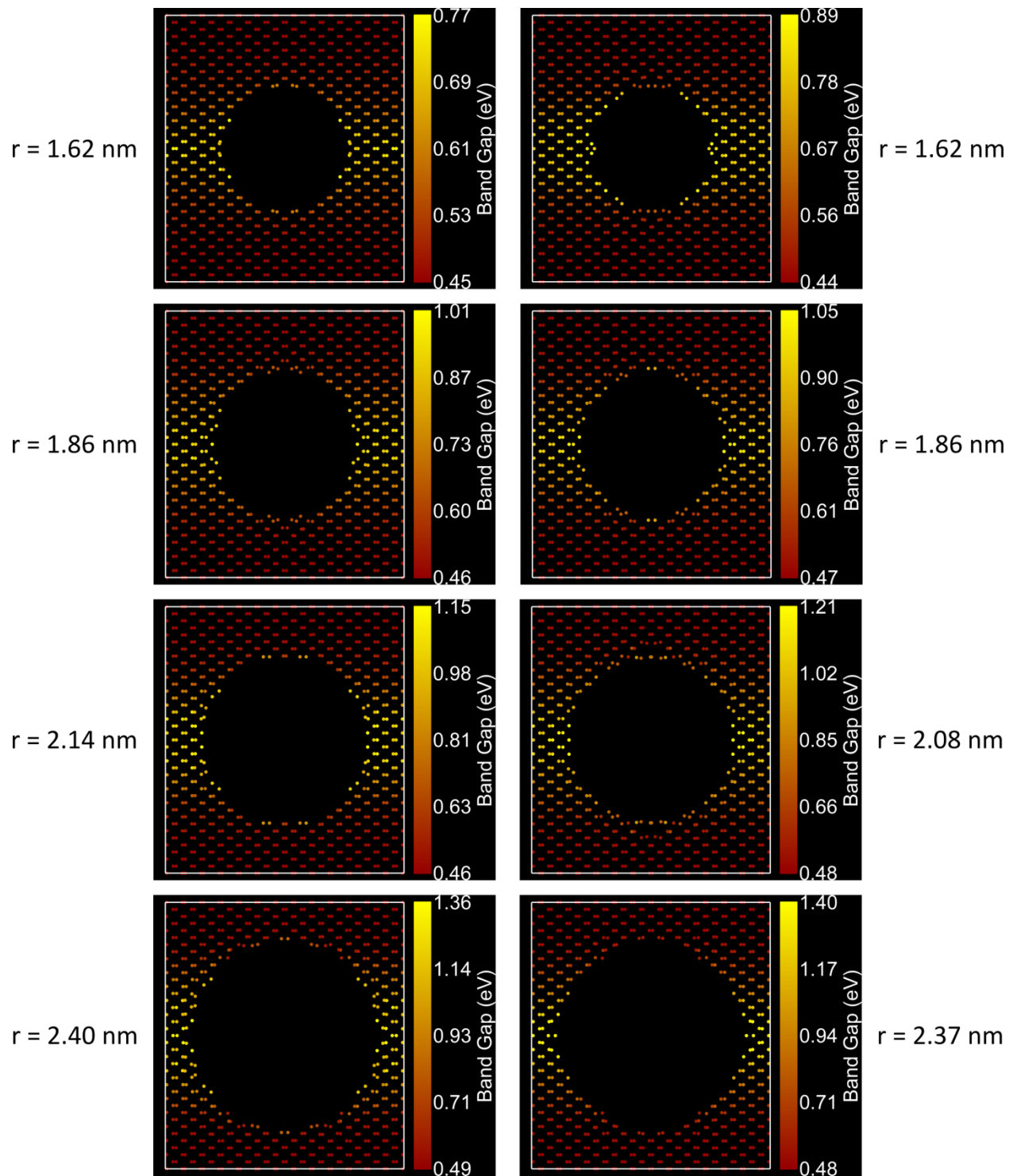


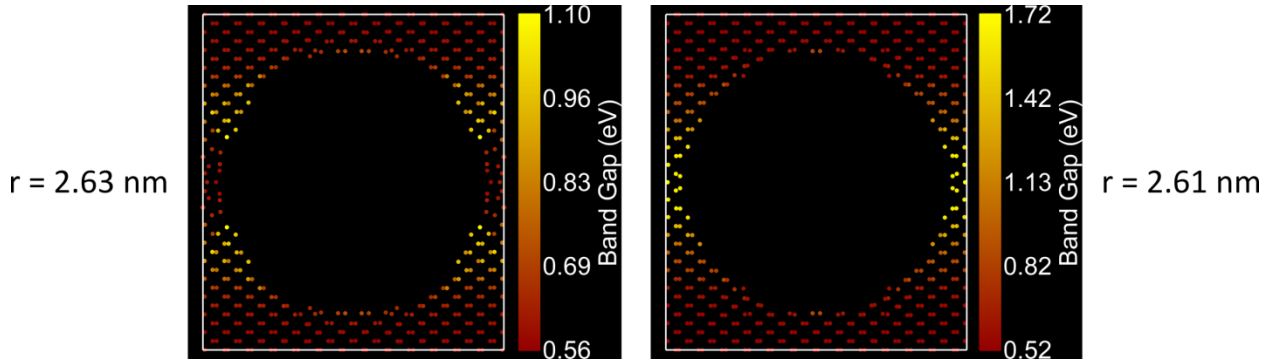












Section S10: Calculated power spectra

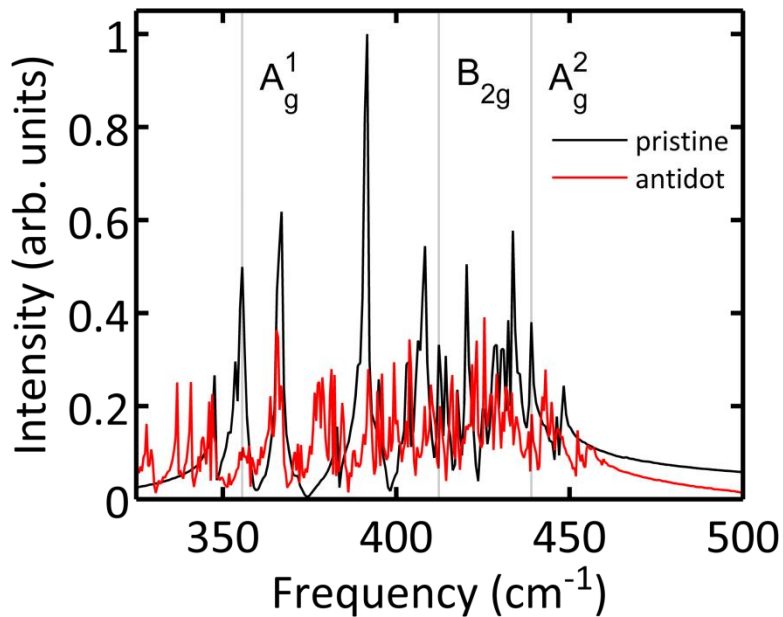


Figure S10. Calculated power spectra for pristine phosphorene (black) and a particular antidot structure (red). Vertical black lines are placed at the Raman active normal modes of interest for the pristine phosphorene.

There are many peaks in the power spectrum since the Raman selection rules are not available in this method. To identify the Raman active peaks of interest for the pristine material the Phonopy values are used in coordination with experimental information on the temperature shifts.¹ The linear $d\omega/dT$ coefficients are used to estimate the frequency shifts for each mode for a change in temperature from 0 K to 300 K. For A_g^1 , B_{2g} , and A_g^2 the frequency shifts are about -2.19, -3.90, and -3.60 cm^{-1} , respectively. Note that these will be overestimates since $d\omega/dT$ is expected to go to zero as 0 K is approached (at low temperatures the amplitude is reduced and the atoms access a potential which is more and more harmonic). Extrapolation is required outside of the experimental range (123 K to 303 K) to make these estimates. The lower bounds for the frequencies for A_g^1 , B_{2g} , and A_g^2 are then 354.2, 412.2, and 437.6 cm^{-1} respectively. Finally, the frequencies for A_g^1 , B_{2g} , and A_g^2 can be identified in the power spectrum as 355.6, 412.3, and

439.0 cm^{-1} . Subsequently the antidot frequencies can be determined to be between 354.9 and 357.5 cm^{-1} for A_g^1 , and at 412.6 and 439.1 cm^{-1} for B_{2g} and A_g^2 , respectively.

Section S11: Justification for neglecting spin-polarization

The calculations performed in this study did not include spin-polarization and an analysis of the literature indicates that this is justified. ZZ-1 PNRs with bare^{5, 3} and O-passivated² edges host an edge-edge antiferromagnetic state, while the H-terminated case is non-magnetic.² AC and ZZ-1 phosphorene NRs display an edge-edge antiferromagnetic state when passivated by H+O and O+OH, but not for termination by H+H, O+O, OH+OH, H+O, H+OH, and O+OH (including bare edge). The ZZ-2 edge did not host any magnetic properties for these edge dopants (including bare edge).⁴ The notation A+B means that there are two edge atoms in the unit cell for each end of the NR, where one atom is passivated by A and the other by B. Self-passivated and H- or F-passivated diagonal PNRs are non-magnetic.⁵ The edge-edge AFM state only emerges in diagonal PNRs with bare edges⁵ and O-passivation.^{5, 6} In general magnetic properties result from the presence of dangling bond(s) at the edge.² Since all of the phosphorus dangling bonds are hydrogen-passivated, it is reasonable to neglect spin-polarization effects in this first study despite the fact that there are many edge configurations that have not been studied separately. Future work could assess spin-polarization effects in PALs, either by leaving the dangling bonds unpassivated or by passivating with oxygen (which is experimentally likely) so that dangling bonds remain.

References

- (1) Ling, X.; Liang, L.; Huang, S.; Puretzky, A. A.; Geohegan, D. B.; Sumpter, B. G.; Kong, J.; Meunier, V.; Dresselhaus, M. S. Low-Frequency Interlayer Breathing Modes in Few-Layer Black Phosphorus. *Nano Lett.* **2015**, *15*, 4080-4088.
- (2) Zhu, Z.; Li, C.; Yu, W.; Chang, D.; Sun, Q.; Jia, Y. Magnetism of Zigzag Edge Phosphorene Nanoribbons. *Appl. Phys. Lett.* **2014**, *105*, 113105.
- (3) Du, Y. P.; Liu, H.; Xu, B.; Sheng, L.; Yin, J.; Duan, C.-G.; Wan, X. Unexpected Magnetic Semiconductor Behavior in Zigzag Phosphorene Nanoribbons Driven by Half-Filled One Dimensional Band. *Sci. Rep.* **2015**, *5*, 8921.
- (4) Ding, B.; Chen, W.; Tang, Z.; Zhang, J. Tuning Phosphorene Nanoribbon Electronic Structure through Edge Oxidation. *J. Phys. Chem. C* **2016**, *120*, 2149-2158.
- (5) Farooq, M. U.; Hashmi, A.; Hong, J. Ferromagnetism Controlled by Electric field in Tilted Phosphorene Nanoribbon. *Sci. Rep.* **2016**, *6*, 26300.
- (6) Zhang, S.; Li, C.; Guo, Z. X.; Cho, J.-H.; Su, W.-S.; Jia, Y. Magnetic Evolution and Anomalous Wilson Transition in Diagonal Phosphorene Nanoribbons Driven by Strain. *Nanotechnology* **2015**, *26*, 295402.